JEM Journal of Experimental Medicine

BRIEF DEFINITIVE REPORT

Dysregulation of sphingolipid metabolism contributes to bortezomib-induced neuropathic pain

Katherine Stockstill[1], Timothy M. Doyle[1], Xisheng Yan[2], Zhoumou Chen[1], Kali Janes[1], Joshua W. Little[1,3], Kathryn Braden[1], Filomena Lauro[1], Luigino Antonio Giancotti[1], Caron Mitsue Harada[1], Ruchi Yadav[2], Wen Hua Xiao[4], Jack M. Lionberger[5], William L. Neumann[6], Gary J. Bennett[4], Han-Rong Weng[2], Sarah Spiegel[7], and Daniela Salvemini[1]

The development of chemotherapy-induced painful peripheral neuropathy is a major dose-limiting side effect of many chemotherapeutics, including bortezomib, but the mechanisms remain poorly understood. We now report that bortezomib causes the dysregulation of de novo sphingolipid metabolism in the spinal cord dorsal horn to increase the levels of sphingosine-1-phosphate (S1P) receptor 1 (S1PR1) ligands, S1P and dihydro-S1P. Accordingly, genetic and pharmacological disruption of S1PR1 with multiple S1PR1 antagonists, including FTY720, blocked and reversed neuropathic pain. Mice with astrocyte-specific alterations of *S1pr1* did not develop neuropathic pain and lost their ability to respond to S1PR1 inhibition, strongly implicating astrocytes as a primary cellular substrate for S1PR1 activity. At the molecular level, S1PR1 engaged astrocyte-driven neuroinflammation and altered glutamatergic homeostasis, processes blocked by S1PR1 antagonism. Our findings establish S1PR1 as a target for therapeutic intervention and provide insight into cellular and molecular pathways. As FTY720 also shows promising anticancer potential and is FDA approved, rapid clinical translation of our findings is anticipated.

Introduction

Bortezomib (Velcade) is a dipeptide boronic acid inhibitor of the 26S proteasome widely used in the treatment of multiple myeloma and mantle cell non-Hodgkin's lymphoma (Chen et al., 2011). More than 40% of patients receiving bortezomib develop chronic, distal, and symmetrical sensory peripheral neuropathy often accompanied by a neuropathic pain syndrome (chemotherapy-induced painful peripheral neuropathy [CIPN]) that may last for weeks, months, or even years after drug termination (Farquhar-Smith, 2011). CIPN greatly compromises the quality of life of cancer survivors and patients under treatment and can interfere with effective anticancer treatment (Farquhar-Smith, 2011). Dose reduction or treatment discontinuation is often the sole recourse for patients who develop neuropathic pain, because traditional analgesics are ineffective or have their own serious unwanted side effects (Farquhar-Smith, 2011). Advances in strategies to address this growing problem are urgently needed with increased efficacy of cancer therapy that has resulted in nearly 14 million cancer survivors in the United States (de Moor et al., 2013), many suffering from these long-term side effects (Farquhar-Smith, 2011). The mechanisms underlying CIPN remain poorly understood and differ among the chemotherapeutic agents (Han and Smith, 2013). However, neuropathological changes in the dorsal horn of the spinal cord (DHSC) have been documented (Han and Smith, 2013).

As a desirable anticancer mechanism, bortezomib activates the sphingolipid biosynthesis pathway to produce the potent proapoptotic sphingolipid ceramide (Gong et al., 2014). Ceramide is hydrolyzed by ceramidases to sphingosine that is phosphorylated by sphingosine kinases (SphK1 and 2) to produce sphingosine-1-phosphate (S1P; Spiegel and Milstien, 2011). S1P initiates signaling through a family of five cognate G protein–coupled receptors (S1PR1–5; Spiegel and Milstien, 2011) and, in contrast to ceramide, is a potent antiapoptotic sphingolipid (Ogretmen and Hannun, 2004). It is hypothesized that the ceramide/S1P rheostat plays a critical role in regulating cancer cell fate with elevated levels of ceramide inducing cell death and elevated

[1]Department of Pharmacology and Physiology, Saint Louis University School of Medicine, St. Louis, MO; [2]Department of Pharmaceutical and Biomedical Sciences, College of Pharmacy, University of Georgia, Athens, GA; [3]Department of Surgery, Center for Anatomical Science and Education, Saint Louis University School of Medicine, St. Louis, MO; [4]Department of Anesthesiology, University of California, San Diego, La Jolla, CA; [5]Department of Internal Medicine, Division of Hematology, Oncology, and Cellular Therapeutics, Saint Louis University School of Medicine, St. Louis, MO; [6]Department of Pharmaceutical Sciences, School of Pharmacy, Southern Illinois University Edwardsville, Edwardsville, IL; [7]Department of Biochemistry and Molecular Biology, Virginia Commonwealth University, School of Medicine, Richmond, VA.

Correspondence to Daniela Salvemini: daniela.salvemini@health.slu.edu.

levels of S1P leading to survival and proliferation (Ogretmen and Hannun, 2004). Thus, therapeutic strategies aimed at reducing S1P bioavailability or signaling are attracting attention as novel anticancer agents (Ogretmen and Hannun, 2004). Numerous studies have demonstrated that the S1PR1 functional antagonist and orally available multiple sclerosis drug FTY720 (fingolimod; Gilenya; Brinkmann et al., 2010) has potent antitumor activity (Hait et al., 2015; White et al., 2016) and can synergize with bortezomib to target multiple myeloma cells in vitro and multiple myeloma in vivo xenografts (Beider et al., 2017).

Despite having opposing effects on cancer cells, compelling evidence is emerging that ceramide and S1P share potent inflammatory and nociceptive actions (Salvemini et al., 2013). It is noteworthy that altered sphingolipid metabolism caused by mutations in serine palmitoyltransferase (SPT) contributes to neuropathic pain in humans (Dawkins et al., 2001). Whether sphingolipid dysregulation drives bortezomib-induced neuropathic pain is not known. Here, we demonstrate that S1PR1-dependent neuroinflammatory signaling pathways contribute to the development of bortezomib-induced neuropathic pain identifying S1PR1 as a molecular target for therapeutic intervention.

Results and discussion

Dysregulation of sphingolipid metabolism by bortezomib

Bioactive sphingolipid metabolites are powerful signaling molecules, and minor changes are known to have significant impact in signal transduction (Hannun and Obeid, 2008). Liquid chromatography–electrospray ionization–tandem mass spectrometry (LC-ESI-MS/MS) analysis of multiple sphingolipid species (Fig. 1 A) revealed that bortezomib treatment (Zheng et al., 2012; Janes et al., 2013) caused dysregulation of sphingolipid metabolism in the DHSC. Indeed, bortezomib induced significant increases in the levels of ceramide (Figs. 1 B and S1 A) and its de novo biosynthetic pathway precursors, dihydrosphingosine and dihydroceramide (Figs. 1 B and S1 B). Bortezomib also increased the levels of sphingosine, S1P, and dihydro-S1P (DH-S1P), which are metabolites of ceramide and dihydroceramide (Fig. 1 B). In contrast, there were no observable changes in sphingomyelin (Fig. 1 B). These results suggest that dysregulation of sphingolipid metabolism from the de novo pathway within the DHSC is among the early events of bortezomib-induced neuropathic pain. Dysregulation of sphingolipid metabolism was associated with time-dependent development of neuropathic pain (mechano-allodynia and mechano-hyperalgesia; Figs. 2 and S2). Our sphingolipidomic data supporting the contribution of the de novo pathway in bortezomib-induced neuropathic pain were substantiated with studies performed with myriocin, a well-characterized inhibitor of SPT (Delgado et al., 2006), the first and rate-limiting enzyme of de novo pathway. Myriocin, when used at doses reported to block SPT (Delgado et al., 2006) and S1P levels in DHSC (Muscoli et al., 2010) significantly attenuated the development of neuropathic pain (Fig. 1, C and D). Collectively, the data strongly suggest that bortezomib alters S1P signaling by triggering SPT and de novo sphingolipid metabolism.

Genetic and pharmacological inhibition of the S1PR1 axis mitigates bortezomib-induced neuropathic pain

Because S1P and DH-S1P are potent bioactive mediators and ligands with similar affinities for S1PR1 (Strub et al., 2010), we explored the functional contribution of S1PR1 using NIBR14, a methyl ester prodrug that is rapidly hydrolyzed in vivo to the carboxylic acid, NIBR15, a potent and selective S1PR1 antagonist (Angst et al., 2012). i.th. administration of NIBR14 attenuated the development of mechano-allodynia and mechano-hyperalgesia in rats (Figs. 2 A and S2 A). In support of these pharmacological effects, i.th. administration of *S1pr1*-targeting dicer-substrate short interfering RNA (DsiRNA) during bortezomib treatment recapitulated the pharmacological blockade (Figs. 2 B and S2 B) by significantly reducing S1PR1 protein levels in the DHSC (Fig. 2 C). These data provide convergent evidence that blocking S1PR1 signaling mitigates bortezomib-induced neuropathic pain.

The pharmacological efficacy and potency of oral administration of S1PR1-targeted agents, which is the preferred clinical approach, was examined using S1PR1 competitive (NIBR14) and functional (FTY720, ponesimod) antagonists (Bigaud et al., 2014). FTY720 (once phosphorylated by SphK2 to the biologically active FTY720-P) and ponesimod are S1PR1 agonists that act as "functional antagonists" by potently and irreversibly down-regulating S1PR1 (Bigaud et al., 2014). Oral administration of NIBR14 or FTY720 during bortezomib treatment dose-dependently prevented neuropathic pain from developing for the 20-d observation period after the completion of bortezomib treatment (Figs. 2, D and E; and S2, C and D; ED_{50} values in Table 1). Oral administration of ponesimod exhibited similar beneficial effects (Fig. S2, E and F). The beneficial effects observed with FTY720 were independently verified by another laboratory in our group using another method of behavioral assessment (Fig. 2, F and G).

Numerous studies have convincingly demonstrated the antitumor effects of FTY720 on many types of cancer cells in vitro and in tumor-bearing animals (Yasui et al., 2005; Alinari et al., 2011; Neviani et al., 2013; Hait et al., 2015). Therefore, S1PR1 agents are not expected to reduce the chemotherapeutic effectiveness of bortezomib. We confirmed this with in vitro tumor cell–killing studies using FTY720. Based on pharmacokinetic studies in rats (Brinkmann et al., 2010), the anticipated plasma levels of FTY720 at doses providing maximal blockade of bortezomib-induced neuropathic pain are ∼0.5–0.7 nM. When tested at a much higher dose, FTY720 (5 µM) did not significantly diminish the in vitro tumor cell toxicity of bortezomib in human multiple myeloma (RPMI 8226) cells (LC_{50}, 34 nM; 95% confidence interval [CI], 27–42 nM; $n = 5$) compared with bortezomib and vehicle (LC_{50}, 31 nM; 95% CI, 23–42 nM; $n = 5$).

Astrocytes are a primary cellular substrate for S1PR1 activity after bortezomib treatment

In the central nervous system (CNS), astrocytes express much higher levels of S1PR1 than microglia and neurons (Zhang et al., 2014), marking these cells as a prime target for S1PR1 signaling in the development of bortezomib-induced neuropathic pain. To test this possibility, we used mice with floxed *S1pr1* recombined with a *cre* gene under the control of a *glial fibrillary acidic protein* (*Gfap*) promoter that results in the deletion of *S1pr1* in GFAP$^+$

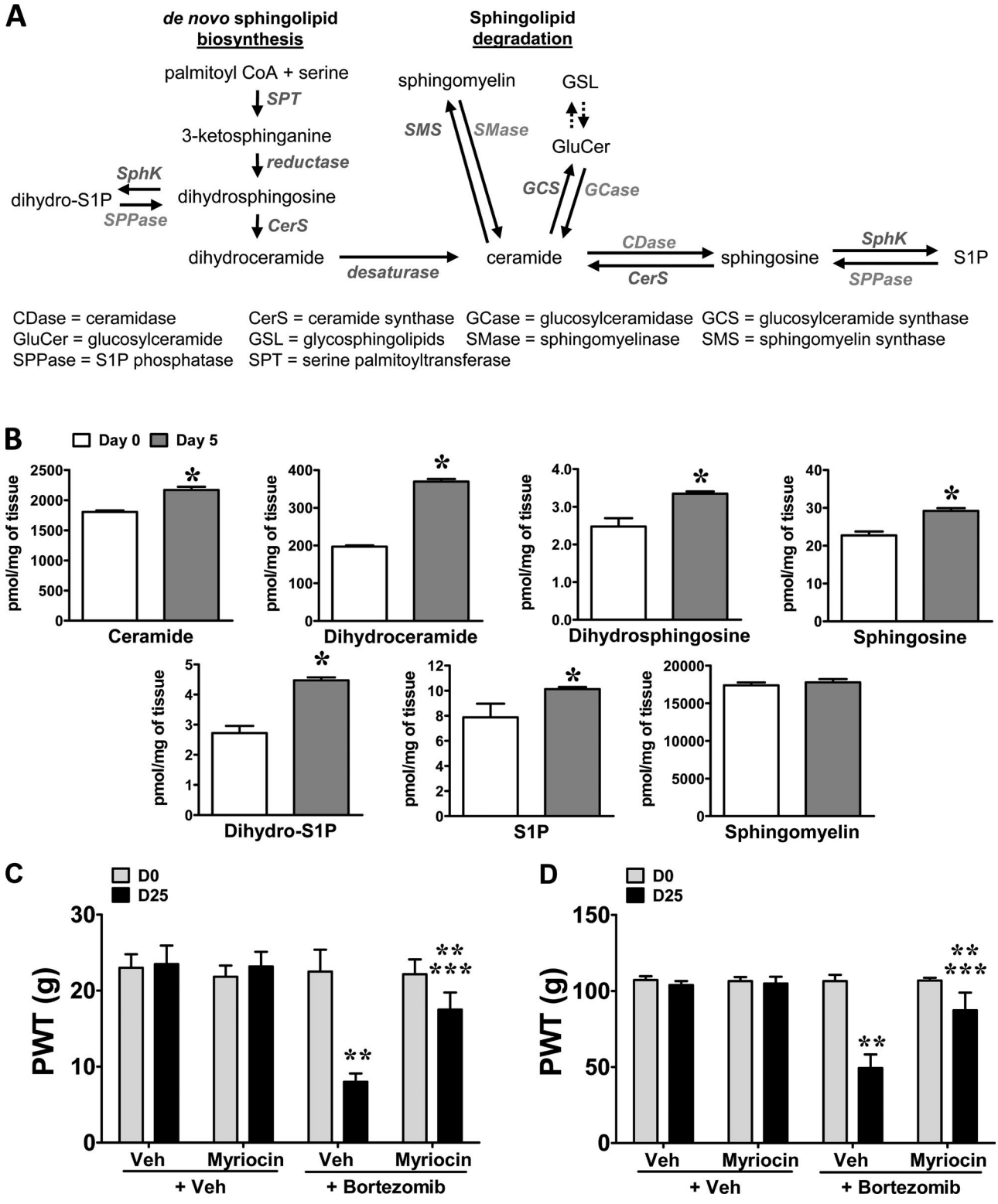

Figure 1. **Bortezomib-induced neuropathic pain is dependent on increased de novo biosynthesis of ceramide and its metabolites in the lumbar DHSC. (A)** Sphingolipid metabolic pathway. **(B)** Extracted lumbar DHSC lipids of rats treated with saline (day 0) or bortezomib (24 h after the last bortezomib injection; day 5) were analyzed by LC-ESI-MS/MS (n = 4 per group; representative of two separate experiments). **(C and D)** Mechano-allodynia (C) and mechano-hyperalgesia (D) were measured in rats (n = 6 per group) treated on days 0–4 with bortezomib or vehicle and concurrent i.th. delivery of myriocin (0.3 µM/d) or its vehicle. Data are mean ± SD for n rats; (B) *, $P < 0.05$ versus day 0 by Welch's corrected, unpaired, one-tailed Student's t test and (C) **, $P < 0.05$ versus day 0 and ***, $P < 0.05$ versus time-matched bortezomib plus vehicle by one-way ANOVA with Holm-Sidak. False discovery rate was controlled by Benjamini-Hochberg procedure (B: $q < 0.05$; $q^* = 0.027$).

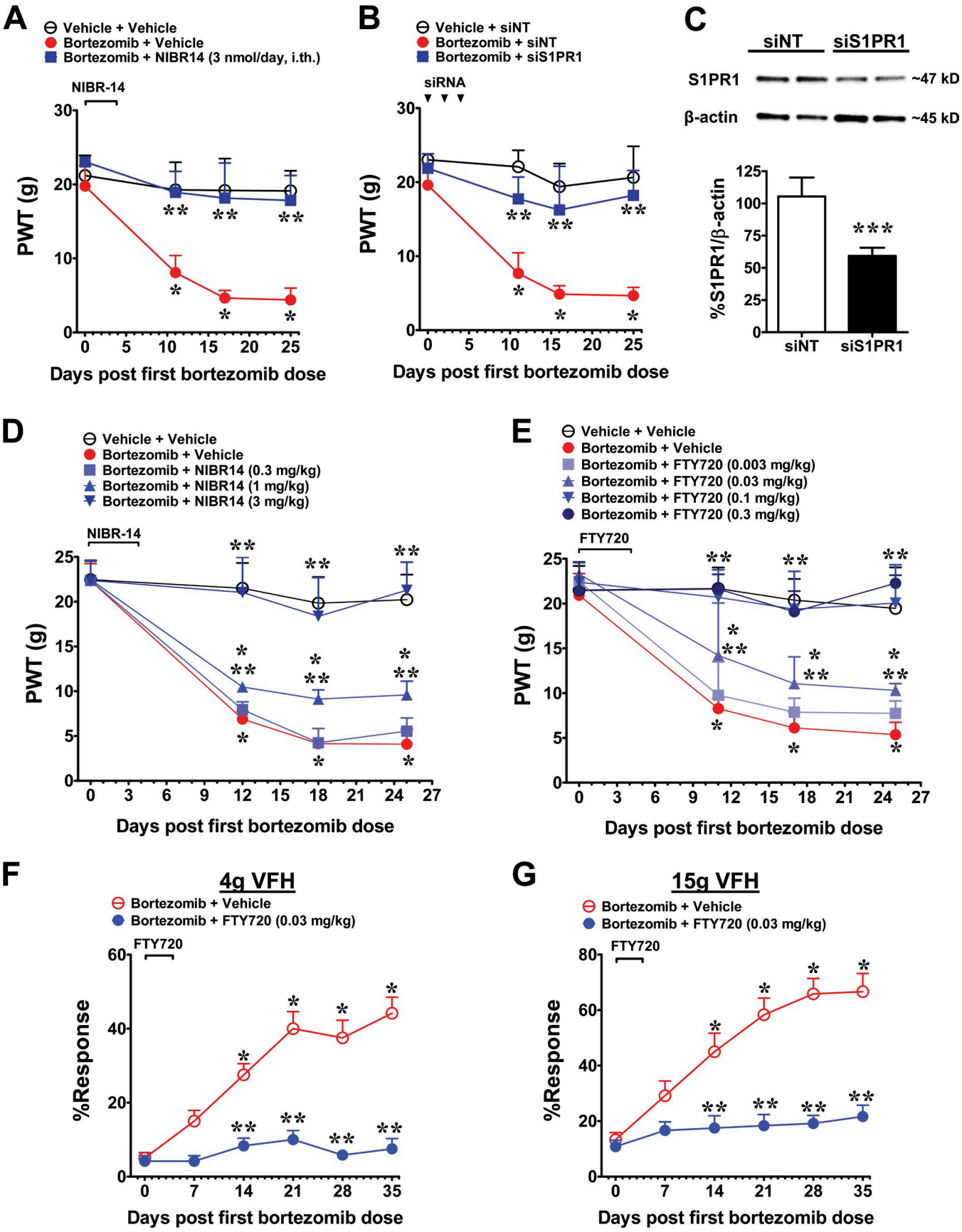

astrocytes in the CNS (Choi et al., 2011). We confirmed the deletion of *S1pr1* in the spinal cord (Fig. 3, A and B) and intact *S1pr1* in dorsal root ganglion (DRG) tissues (Fig. 3 A). When compared with control littermates, male mice with astrocyte-specific deletions of *S1pr1* did not develop neuropathic pain (Fig. 3 C). In animal models of multiple sclerosis, Choi et al. (2011) demonstrated that these mice develop a lesser form of the disease while losing the ability to respond to FTY720. Because in our pain model the complete deletion of *S1pr1* from astrocytes resulted in no development of pain, we used mice with astrocyte-specific reductions of *S1pr1* to examine the role of *S1pr1* in astrocytes on the pharmacological effects of S1PR1 antagonists. Mice with astrocyte-specific reductions of *S1pr1* had delayed development of neuropathic pain compared with controls and, because of reduced levels of S1PR1, they also lost their responsiveness to the beneficial effects of FTY720 (Fig. 3 D). These data, which mimic those obtained with S1PR1 antagonists and siRNA, strongly suggest that activation S1PR1 signaling in astrocytes is necessary for both bortezomib-induced neuropathic pain and the analgesic effects of FTY720, thus identifying astrocytes as a primary cellular substrate of S1PR1 activity.

S1PR1-driven neuroinflammation contributes to bortezomib-induced neuropathic pain

Bortezomib-induced dysregulation of sphingolipid metabolism in the spinal cord was associated with increased levels of the astrocyte marker GFAP (Fig. 4, A–D and G) in the superficial dorsal horn (laminae I and II), confirming a previous study (Robinson et al., 2014). The increase in GFAP suggests an increase in the number of astrocytes, their activation, or both in the DHSC in response to bortezomib. S1P triggers astrocytes to become reactive (Sorensen et al., 2003), and activation of S1PR1 can induce astrocyte migration in culture (Mullershausen et al., 2007). In other neurodegenerative diseases with a prominent astrocyte-driven inflammatory component (e.g., multiple sclerosis, Alzheimer's disease, or Huntington's disease), blocking the S1PR1 axis with S1PR1 antagonists attenuates astrocyte activation and inhibits increased production of inflammatory cytokines in the spinal cord; in contrast, levels of IL-10 increase (Brinkmann et al., 2010; O'Sullivan and Dev, 2017). These antiinflammatory effects of S1PR1 antagonism are further supported by a recent study showing that FTY720 can prevent endotoxin activation, migration, and ensuing release of inflammatory mediators in primary astrocyte cultures, but not microglia (Rothhammer et al., 2017). In our study, bortezomib-induced dysregulation of sphingolipid metabolism was also associated with concomitant increases in TNF and IL-1β (Fig. 4, H and I). In contrast, antiinflammatory cytokines (IL-10 and IL-4) decreased compared with those in vehicle-treated rats (Fig. 4, J and K). Concurrent administration of FTY720 attenuated increased GFAP immunolabeling (Fig. 4, E–G) and production of TNF and IL-1β (Fig. 4, H and I) associated with bortezomib treatment while preventing reductions in IL10 and IL4 (Fig. 4, J and K). Similar effects on cytokine expression were obtained with ponesimod (Fig. 4, H–K). This S1PR1-driven neuroinflammation in the spinal cord may, in turn, establish "feed-forward" mechanisms that can sustain dysregulation of sphingolipid metabolism. For example, TNF and IL-1β can activate the major enzymes involved in the biosynthesis of ceramide and S1P pathways: SphK1, sphingomyelinases, SPT, and ceramidases (Snider et al., 2010). Interruption of this cross talk early in the bortezomib regimen may explain how neuropathic pain is prevented with S1PR1-targeted agents from developing for many days after bortezomib discontinuation (Figs. 2 and S2).

Table 1. **Analgesic ED_{50} values for oral administration of NIBR14 or FTY720 in bortezomib-induced neuropathic pain (day 25)**

Treatment	Pain behavior	ED_{50}	95% CI	*n*
		μmol/kg		
NIBR14	Allodynia	2	1–3	6
	Hyperalgesia	2	1–3	6
FTY720	Allodynia	0.09	0.06–0.2	3–11
	Hyperalgesia	0.09	0.06–0.1	3–11

S1PR1-driven alterations in glutamatergic signaling

Spinal synaptic mechanisms underlying the development of bortezomib-induced neuropathic pain have not been identified. We investigated whether glutamatergic synaptic activities in the DHSC of rats with bortezomib-induced neuropathic pain were altered using whole-cell patch-clamp recording techniques. Miniature excitatory postsynaptic currents (mEPSCs) were recorded from neurons in the spinal outer lamina II receiving monosynaptic input from the primary afferents (Yoshimura and Jessell, 1989; Weng et al., 2006). Alterations in mEPSC frequency indicate changes in the presynaptic transmitter release probability, whereas alteration in mEPSC amplitude indicates changes in the postsynaptic glutamate receptor function (Lissin et al., 1999; Yan et al., 2013; Yan and Weng, 2013). We found that

Figure 2. **Inhibition of S1PR1 prevents bortezomib-induced neuropathic pain. (A)** Mechano-allodynia measured in rats treated with the vehicles of bortezomib and NIBR14 (*n* = 6) or with bortezomib and concurrent i.th. NIBR14 (3 nmol/d, days 0–4; *n* = 6) or vehicle (10% DMSO; *n* = 6). **(B)** Mechano-allodynia was measured in rats treated on days 0–4 with bortezomib vehicle and nontargeting DsiRNA (siNT; *n* = 6) or with bortezomib and concurrent i.th. *S1pr1*-targeting (siS1PR1) DsiRNA or siNT (2 μg/d on days 0, 2, and 4; *n* = 6 per group). Pilot studies showed that i.th. NIBR14 or *S1pr1*-targeting DsiRNA had no effect on PWT in vehicle-treated rats (not depicted). **(C)** Representative blots showing S1PR1 protein in DHSC from rats receiving siS1PR1 (*n* = 3) or siNT (*n* = 3). **(D and E)** Mechano-allodynia was measured in rats treated with bortezomib vehicle and test agent vehicle (*n* = 6 in D; *n* = 9 in E) or with bortezomib (days 0–4) and concurrent oral NIBR14 (0.3, 1, or 3 mg/kg/d; *n* = 6 per group in D), oral FTY720 (0.003, 0.03, or 0.1 mg/kg/d; *n* = 6 per group; or 0.3 mg/kg/d; *n* = 3 in E), or their vehicles (10 or 2% DMSO in saline; *n* = 7 in D; or *n* = 11 in E). **(F and G)** Mechano-hypersensitivity was measured in rats treated with bortezomib and concurrent oral FTY720 (0.03 mg/kg/d; *n* = 12) or its vehicle (*n* = 12) by an independent laboratory in our group by using a previously reported von Frey method (Siau et al., 2006). Data are mean ± SD (A–E) or mean ± SEM (F and G) for *n* rats; *, P < 0.05 versus day 0; **, P < 0.05 versus time-matched bortezomib plus vehicle or bortezomib plus siNT; ***, P < 0.05 versus siNT by two-way ANOVA with Holm-Sidak (A, B, and D–G) or Student's *t* test (C).

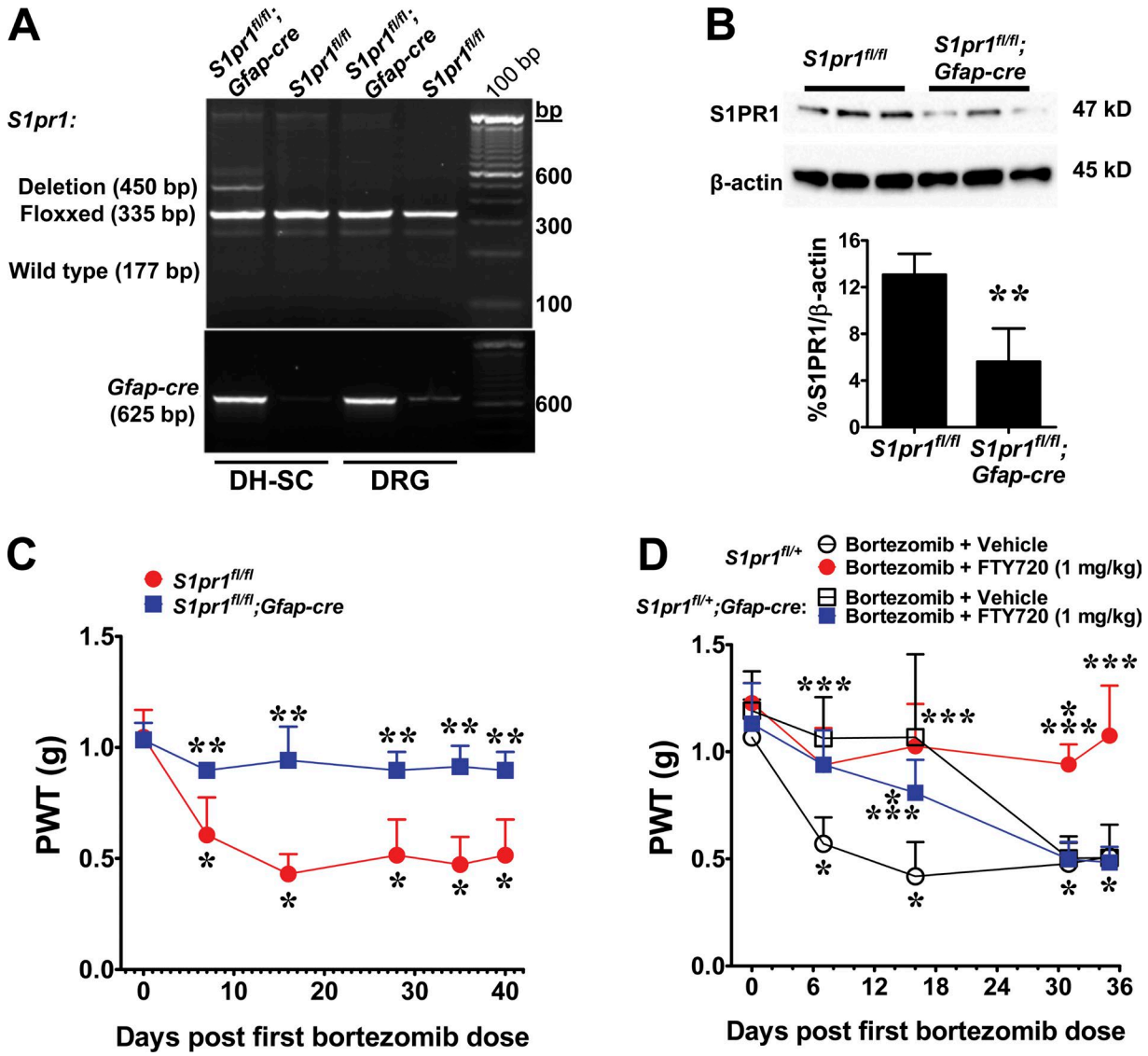

Figure 3. **Astrocytes are cellular targets of S1PR1 activity in the spinal cord. (A)** Representative image of DNA PCR of spinal cords and DRGs from naive mice with astrocyte-specific *S1pr1* deletion (*S1pr1*$^{fl/fl}$;*Gfap-Cre*; $n = 3$) or their controls (*S1pr1*$^{fl/fl}$; $n = 3$). Assays were repeated twice on different days. **(B)** S1PR1 Western blot in the spinal cord of mice ($n = 3$ per group; performed twice on different days). **(C)** Mechano-allodynia was measured in bortezomib-treated male mice with astrocyte-specific deletions of *S1pr1* ($n = 7$) and their controls ($n = 5$). **(D)** Mechano-allodynia was measured in mice with astrocyte-specific reductions in *S1pr1* and their controls treated concurrently with bortezomib and i.p. vehicle ($n = 7$ per group) or FTY720 (1 mg/kg; *S1pr1*$^{fl/+}$: $n = 7$, *S1pr1*$^{fl/+}$;*Gfap-Cre*: $n = 6$). Data are mean ± SD for n mice; *, $P < 0.05$ versus day 0; **, $P < 0.05$ versus time-matched *S1pr1*$^{fl/fl}$ mice; and ***, $P < 0.05$ versus *S1pr1*$^{fl/+}$ with bortezomib plus vehicle by Student's t test (B) or two-way ANOVA with Holm-Sidak (C and D).

both the frequency (6.10 ± 0.44 Hz) and amplitude (26.37 ± 0.52 pA) of mEPSCs in neurons from rats with bortezomib-induced neuropathic pain were significantly higher ($P < 0.0001$, Welch's uncorrected t test) than in vehicle-treated rats (frequency, 3.14 ± 0.33 Hz; amplitude, 22.87 ± 0.77 pA), suggesting that glutamate release from presynaptic terminals and ligand-gated glutamate receptor function in postsynaptic neurons are enhanced in bortezomib-treated rats (Fig. 4, L–O).

Previous studies by others and us have shown that spinal glutamatergic synaptic activities are enhanced by inflammatory mediators (e.g., TNF, IL-1β, and MCP1) under pathological pain conditions (Kawasaki et al., 2008; Yan and Weng, 2013). However, their regulation by the S1PR1 axis is not known. NIBR15 treatment significantly reduced the mEPSC frequency, but not amplitude, from 6.10 ± 0.44 Hz to 4.09 ± 0.23 Hz (Fig. 4, L and N) in DHSC neurons from rats with bortezomib-induced neuropathic pain. Furthermore, perfusion of the selective S1PR1 agonist SEW2871 in normal rats significantly increased mEPSC frequency with no significant change in amplitude (Fig. 4, M and O). Collectively, these data suggest that S1P in the DHSC of bortezomib-treated rats enhances glutamate release from presynaptic terminals, which is blocked by S1PR1-targeted agents.

These findings demonstrate the dysregulation of excitatory glutamatergic signaling as a second factor contributing to neuropathic pain induced by chemotherapeutics (Boyette-Davis et al., 2015). More importantly, our study demonstrates for the first

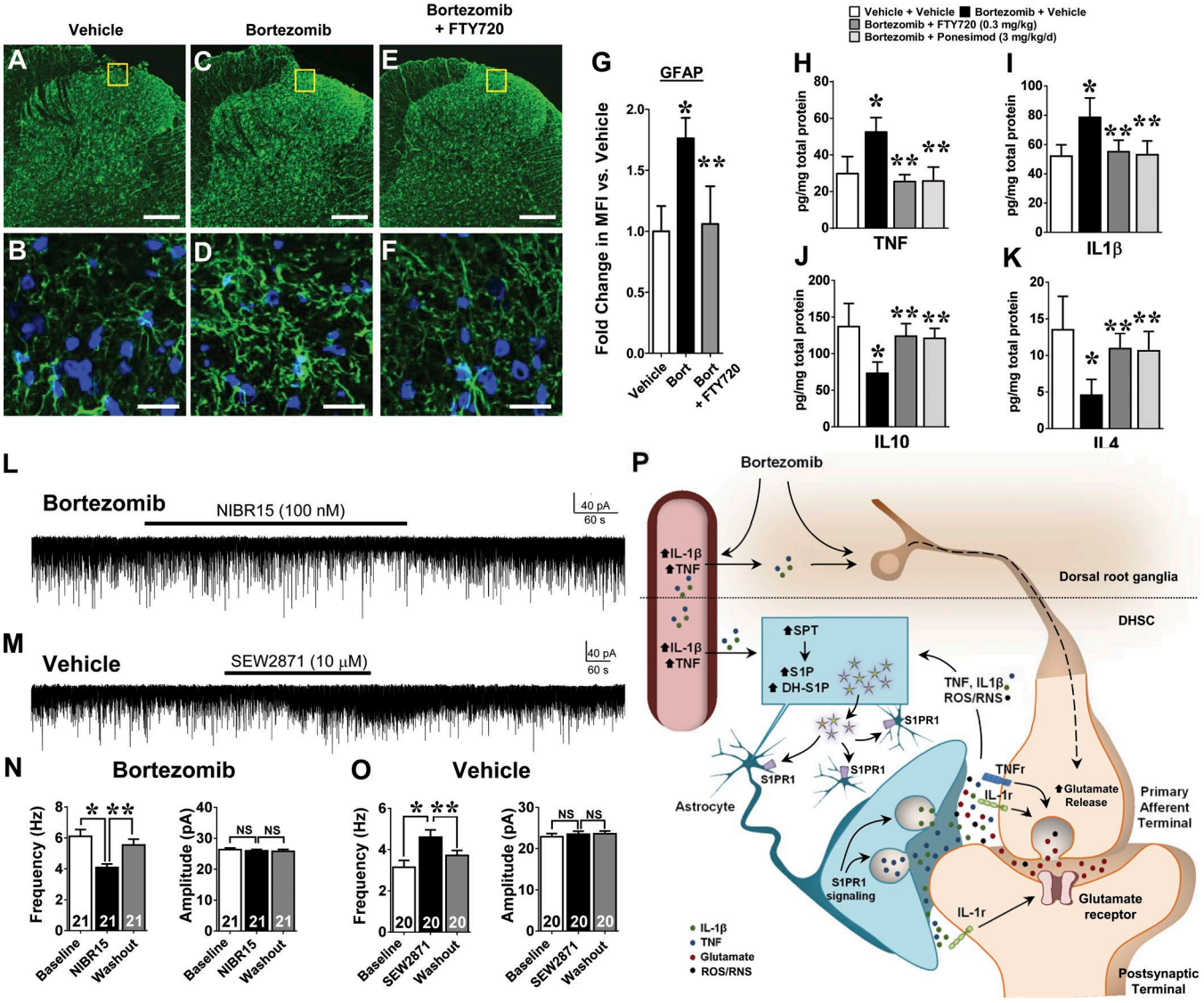

Figure 4. **FTY720 attenuated bortezomib-induced astrocyte activation, neuroinflammation, and enhancement of presynaptic glutamate release in the DHSC. (A–F)** Lumbar DHSC from rats treated with vehicle (A and B), bortezomib (C and D) or bortezomib plus FTY720 (0.3 mg/kg/d, oral; E and F) were harvested at day 25 (peak mechano-allodynia) and immunolabeled for GFAP (green) with DAPI staining (blue). Isotypic antibody controls exhibited low levels of background fluorescence (not depicted). Representative micrographs are from the L4 level (three bilateral sections per animal from L4, L5, and L6 DHSC levels; A, C, and E; bars, 250 µm) and magnified sections in B, D, and F (bars, 20 µm) are demarcated by yellow boxes. **(G)** Quantitative fold change in MFI versus vehicle (n = 3 per group) for GFAP signal in laminae I and II of the superficial DHSC. **(H–K)** Cytokine levels in DHSC (n = 6 per group) harvested on day 25 from rats treated with vehicles to bortezomib and test agents (oral, n = 6) or bortezomib and oral vehicle, FTY720 (0.3 mg/kg/d) or ponesimod (3 mg/kg/d). **(L and M)** Representative mEPSCs recording on day 7 from bortezomib-treated rats before (baseline), during, and after washout of NIBR15 (100 nM; L) or vehicle-treated rats before, during, and after washout of SEW2871 (10 µM; Chi and Nicol, 2010; M). **(N and O)** Mean mEPSC frequencies and amplitudes before, during, and after washout of each tested agent in bortezomib- (N) or vehicle-treated rats (O). **(P)** Cartoon depicting proposed mechanism(s) of bortezomib-triggered dysregulation of sphingolipid metabolism in the DHSC. Data are mean ± SD for n rats (G–K) or mean ± SEM for n neurons (shown in each bar; N and O); *, P < 0.05 versus vehicle plus vehicle (G–K) or baseline (N and O); **, P < 0.05 versus bortezomib plus vehicle (G–K) or test agent (N and O) by one-way ANOVA with Holm-Sidak (G–K) or Welch's corrected t test (N and O).

time that S1PR1 signaling is responsible for increased presynaptic glutamate release and the genesis of bortezomib-induced neuropathic pain. Because we found that the development of neuropathic pain is lost when S1PR1 is deleted in astrocytes (Fig. 3 C) and FTY720 lost its effectiveness when S1PR1 is reduced in astrocytes (Fig. 3 D), it is likely that S1PR1-targeted agents suppress astrocyte activity and ensuing neuroinflammation (Rothhammer et al., 2017), attenuating the ability of proinflammatory cytokines to enhance glutamatergic synaptic activity (Clark et al., 2013).

S1PR1-targeted agents reverse bortezomib-induced neuropathic pain

The increased efficacy of cancer therapy has led to nearly 14 million cancer survivors in the United States (de Moor et al., 2013). Many of these survivors continue to suffer from long-term neuropathic pain states that are poorly managed. To address this major unmet medical need, we examined the effectiveness of targeting S1PR1 in models of established bortezomib-induced neuropathic pain. At the time of peak pain (day 25), subcutaneous

minipump infusions of FYT720, ponesimod, or NIBR14 over 6 d (Janes et al., 2014) completely reversed neuropathic pain (Fig. S3) throughout the entire period of drug infusion.

The mechanisms of bortezomib dysregulation of sphingolipid metabolism are not known, but several possibilities are envisioned (Fig. 4 P). The limited ability of bortezomib to cross the blood–brain barrier (Adams et al., 1999) suggests that sphingolipid metabolism in the CNS may be triggered by peripheral inflammatory changes (Seruga et al., 2008). Accordingly, bortezomib increases levels of various proinflammatory cytokines, such as TNF and IL-1β (Liang et al., 2014), in plasma that gain access to the CNS (Yarlagadda et al., 2009) and activate de novo biosynthesis to increase DH-S1P and S1P (Snider et al., 2010; Maceyka and Spiegel, 2014). Alternatively, bortezomib-induced events in the DRG (Carozzi et al., 2013) may provoke production of reactive oxygen and nitrogen species (Duggett and Flatters, 2017) and release of glutamate (Ghelardini et al., 2014) from presynaptic nerve endings that could activate glial sphingolipid metabolism (Kim et al., 2012). The resulting increased S1PR1 signaling in astrocytes promotes their activation, migration, and ensuing release of inflammatory mediators (Rothhammer et al., 2017) to reinforce neuroinflammation and drive the establishment and maintenance of the neuronal sensitization in the CNS. In turn, enhanced reactive oxygen and nitrogen species or glutamatergic signaling may perpetuate the cycle and transition the DHSC toward a chronic hypersensitized state.

In conclusion, by using a multidisciplinary approach, our studies provide new insight into the underlying S1PR1-driven mechanisms engaged during bortezomib-induced neuropathic pain and establish the foundation for proof-of-concept studies with S1PR1-targeted agents that are already in clinical use (FTY720; Brinkmann et al., 2010) or advanced clinical trials for other indications (ponesimod; Bigaud et al., 2014). Our studies provide a compelling case for the consideration of repurposing FTY720 as an adjuvant to bortezomib for the prevention and treatment of chemotherapy-related neurotoxicity to address an immense unmet medical need.

Materials and methods

Experimental animals

Male Sprague Dawley rats (200–220 g starting weight) were from Harlan Laboratories. For S1pr1 knockout and knockdown mice, transgenic mouse colonies were descendants of original homozygous *S1pr1$^{fl/fl}$;GFAP-Cre* breeder mice gifted to us by J. Chun (The Scripps Research Institute, La Jolla, CA; Choi et al., 2011) and interbred to maintain their homozygosity for the floxed *S1pr1* gene with regular backcrosses with C57BL/6J wild-type mice (Harlan Laboratories) to reduce inbred genetic defects. Prior characterizations of these conditional mutants showed the removal of *S1pr1* from GFAP$^+$ astrocytes in the CNS (Choi et al., 2011). Mice with astrocyte-specific deletion of *S1pr1* (*S1pr1$^{fl/fl}$;GFAP-Cre*) and their control littermates (*S1pr1$^{fl/fl}$*) were generated from mating male *S1pr1$^{fl/fl}$* mice with female *S1pr1$^{fl/fl}$;GFAP-Cre* mice. Mice with astrocyte-specific reductions in *S1pr1* (*S1pr1$^{fl/+}$;GFAP-Cre*) and their control littermates (*S1pr1$^{fl/+}$*) were generated from mating male C57BL/6J wild-type mice with female *S1pr1$^{fl/fl}$;GFAP-Cre* mice. All mice were genotyped before breeding or use in experiments by endpoint PCR of ear-punch DNA. The primers used to detect floxed and deleted *S1pr1* were spb1 (Invitrogen; 5′-TTC TAGCCAAGGCATTGCTCCA-3′), Edg1M/S1pr1 (IDT; 5′-CCTCAG AGTCTGGGTAAATTGT-3′), and b1t1c (Invitrogen; 5′-CACAACCTC CTTCTGATGAA-3′) primers. The primers used to detect *Gfap-cre* were *gfap-cre* forward (5′-ATGGTCTGGCTCCAGGTACC-3′) and cre reverse (5′-CAGCATTGCTGTCACTTGGTC-3′). All mice were ear-tagged for identification, and sex- and age-matched littermate controls were used in all experiments.

Animals were housed two to four per cage (for rats), five per cage (for mice), or single housed after surgery in a controlled environment (12-h light/dark cycle) with food and water available ad libitum. All experiments were conducted with the experimenters blinded to treatment conditions. All experiments were performed in accordance with the guidelines of the International Association for the Study of Pain and the National Institutes of Health and approvals from the Saint Louis University, University of Georgia, and the University of California, San Diego, Institutional Animal Care and Use Committees.

i.th. catheters

i.th. compounds (10 µl) were administered via cannulas made from PE10 tubing (427401; Becton Dickinson) that were chronically implanted in rats by using the L5/L6 lumbar approach as previously described (Little et al., 2012).

Osmotic minipump

Rodents were lightly anesthetized with 3% isoflurane and maintained on 2% isoflurane in 100% O_2. An incision was made in the interscapular region for subcutaneous implantation of primed 7-d osmotic minipumps (Alzet 2001; Alza) that infused 1 µl/h as previously described (Janes et al., 2014). Minipumps were filled according to the manufacturer's specifications with test compounds or their vehicle. Immediately after surgery, i.p. loading doses of test compounds or their vehicle were administered, and minipumps were allowed to deliver test agents for 6 d. After implantation, the animals were singly housed for the remainder of the experiment.

Bortezomib-induced neuropathic pain model

In rats, bortezomib (S1013; Selleck Chemicals) or its vehicle (5% Tween 80, P1754 [Sigma-Aldrich]; 5% ethanol, 493546 [Sigma-Aldrich]; and saline) was administered by i.p. injection in rats on 5 consecutive days (day 0 to day 4; 0.2 mg/kg) at an injection volume of 0.2 ml for a final cumulative dose of 1 mg/kg (Janes et al., 2013). In mice, bortezomib (0.4 mg/kg i.p.) was administered every other day three times per week for 4 wk (day 0 to day 25).

Test compounds

All compounds in the prevention models were administered concurrent with bortezomib at the doses and by the routes described in the text after behavior measurements. For the reversal studies, compounds were administered via osmotic minipumps implanted on D24 or D25. FTY720 (fingolimod) was purchased from Cayman Chemical (162359-56-8). Ponesimod

(ACT-128800, (*Z*,*Z*)-5-[3-chloro-4-((2*R*)-2,3-dihydroxy-propoxy)-benzylidene]-2-propylimino-3-*O*-tolylthiazolidin-4-one) was prepared by Shanghai ChemPartner Co. according to the method of Bolli et al. (2010).

For synthesis of NIBR14, the methyl ester pro-drug, the Novartis competitive antagonist NIBR14 (mol wt = 600.17) was prepared as described in the literature (Angst et al., 2012). Molecular identity was confirmed by LCMS (50–95% acetonitrile in 0.05% TFA over 6 min) performed by using a Waters Alliance SQ 3100 system (positive ion electrospray mode) with an Agilent Eclipse (XDB-C18; 4.6 × 150 mm, 5 µm) column (retention time = 7.15 min; $C_{31}H_{38}ClN_3O_5S$; m/z = 600 [M + H$^+$]).

For synthesis of NIBR15, the methyl ester prodrug NIBR14 (90 mg, 0.15 µmol) was dissolved in 6 ml acetic acid and treated with 1.5 ml of concentrated HCl. This mixture was stirred at 50°C for 12 h and concentrated. Recrystallization from acetonitrile afforded 45 mg (48% yield) NIBR15 HCl salt (mol wt = 622.60), confirmed by LCMS (15–95% acetonitrile in 0.05% TFA over 6 min; retention time = 6.97 min; $C_{30}H_{37}Cl_2N_3O_5S$; m/z = 586 ([M + H$^+$-Cl]$^+$); Angst et al., 2012).

For myriocin, [(2S,3R,4R,6E)-2-Aamino-3,4-dihydroxy-2-(hydroxymethyl)-14-oxo-6-eicosenoic acid] from *Mycelia sterilia* was purchased from Sigma-Aldrich (35891-70-4).

Silencing spinal *S1pr1* with DsiRNA

Commercially available 27-mer duplex DsiRNA targeting common splice forms of *S1pr1/Edg1* transcript (RNC.RNAI.N017301.12.1, GenBank accession no. NM_017301; Integrated DNA Technologies; 5′-rCrCrUrGrUrArCrArArArGrCrArGrArGrUrArCrUrUrCrCTG-3′ and 5′-rCrArGrGrArArGrUrArCrUrCrUrGrCrUrUrUrGrUrArCrArGrGrArU-3′) or its nontargeting control sequence (siNT; Integrated DNA Technologies; DS NC1: 5′-rCrGrUrUrArArUrCrGrCrGrUrArUrArArUrArCrGrCrGrUAT-3′ and 3′-rArUrArCrGrCrGrUrArUrUrArUrArCrGrCrGrArUrUrArArCrGrArC-5′; Walk et al., 2012) were diluted in RNase-free water to 0.2 µg/µl. *S1pr1*-targeting (siS1PR1) or siNT sequence (10 µl) was administered after bortezomib injections via i.th. catheters on days 0, 2, and 4.

Behavioral testing

Baseline behavioral measurements to assess mechano-hypersensitivity were always taken before the daily administration of test substances or their vehicles. Pilot tests to examine the effects of S1PR1 antagonists alone in vehicle-treated rats excluded a potential impact of S1PR1 antagonism on baseline paw withdrawal thresholds (PWTs). Thus, systemic or i.th. injections of FTY720 and NIBR14 did not alter baseline PWTs when given alone at the highest dose used in our manuscript in rats that received the vehicle of bortezomib only. Accordingly, we did not include a vehicle plus S1PR1 antagonist group in our experimental design.

Mechano-allodynia was measured as previously described (Janes et al., 2014). Mechanical PWT in grams [PWT, (g)] was measured using an electronic von Frey test (dynamic plantar aesthesiometer, model 37450; Ugo Basile) with a cutoff set at 50 g in rats or calibrated von Frey filaments (Stoelting; range in mice: 0.07–2.00 g; in rats: 2–26 g) using the "up-and-down" method (Dixon, 1980). Mechano-allodynia was defined as a significant ($P < 0.05$) reduction in mechanical mean absolute PWT (g) at forces that failed to elicit withdrawal responses before chemotherapy treatment (day 0). Mechano-hyperalgesia was measured in the rat hind paw using the Randall and Sellitto paw pressure test as previously described (Janes et al., 2014) by using an analgesiometer (model 37215; Ugo Basile). The nociceptive PWT (g) was measured as the force that caused the rat to withdraw its paw (cutoff set at 250 g). Mechano-hyperalgesia was defined as a significant ($P < 0.05$) reduction in nociceptive PWT (g) compared with withdrawal responses before chemotherapy treatment (day 0). The values from both paws were averaged because chemotherapy-induced neuropathy results in bilateral allodynia and hyperalgesia with no differences between left and right hind PWT (g). The ED_{50} and the corresponding 95% CI were determined from dose responses by curve fitting the percentage of prevention of mechano-allodynia or mechano-hyperalgesia on day 25 using the least sum of square method by a normalized three-parameter, nonlinear analysis (Hill slope = 1) with the use of GraphPad Prism (Release 5.03; GraphPad Software, Inc.). The percentage of prevention = (PWT $(g)_{treatment}$ − mean PWT $(g)_{bortezomib}$)/(mean PWT $(g)_{vehicle}$ − mean PWT $(g)_{bortezomib}$) × 100.

In studies performed by an independent laboratory from our group, behavior was measured by using a previously reported von Frey method (Siau et al., 2006). In brief, 4 and 15 g of von Frey hairs were applied bilaterally to the plantar hind paw five times per side with 1–2 min between successive stimuli, and the percentage of stimuli that elicited a withdrawal reflex was recorded. A significant increase in the number of responses to the 4 g of hair is indicative of mechano-allodynia, and an increase to the 15 g of hair indicates mechano-hyperalgesia.

Sphingolipid analysis by MS

After lipid extraction, sphingolipids were quantified by LC-ESI-MS/MS (4000 QTRAP; AB Sciex) as described previously (Hait et al., 2009).

Western blot

Total protein lysates (rat, 20 µg; mouse, 5 µg) from L4–6 were denatured in Laemmli's buffer, resolved on 4–20% SDS-PAGE, and electrotransferred to nitrocellulose membrane. The membranes were blocked for 1 h in 5% milk in 1× PBS, pH 7.4, with 0.05% Tween 20, probed overnight with rabbit anti–S1PR1 antibody (rat, 1:5,000; mouse, 1:30,000; ab11424; Abcam; and MA/PA1-1040; Thermo Fisher Scientific) and visualized with goat anti–rabbit IgG-horseradish peroxidase (1 h, room temperature [RT], 1:10,000–15,000, 7074; Cell Signaling Technology) and Clarity chemiluminescent reagents (1705061; BioRad). The signal was documented using a ChemiDoc imager (BioRad) and analyzed using ImageLab Software v.5.0 (BioRad). Horseradish peroxidase bound to the membrane was inactivated by two incubations in 30% H_2O_2 at RT for 15 min (Sennepin et al., 2009) and reprobed for β-actin by using mouse anti–β-actin antibody, clone AC-15 (1 h, RT; rat, 1:2,000; mouse, 1:10,000; A5441; Sigma-Aldrich) and goat anti–mouse IgG–horseradish peroxidase (1 h, RT; 1:3,000; 04-18-15; KPL). The density of the S1PR1 band was normalized to the corresponding β-actin band and expressed as percent S1PR1/β-actin.

S1PR1 knockdown PCR

Ear snip, spinal cord, or DRG DNA was isolated by using a QIAmp DNA mini isolation kit (Qiagen) and quantitated by NanoDrop (NanoDrop Products) for PCR as previously described (Choi et al., 2011). In brief, DNA (20–25 ng) was subjected to PCR (25 µl) in duplicate by using two separate PCR reactions: (1) *Edg1M* (*S1pr1*) (5′-CCTCAGAGTCTGGGTAAATTGT-3′; Integrated DNA Technologies), *SPB1* (5′-TTCTAGCCAAGGCATTGCTCCA-3′; Invitrogen), and *B1T1C* (5′-CACAACCTCCTTCTGATGAA-3′; Invitrogen) sites by using the following amplification cycle conditions: 94°C, 5 min; 35 cycles (94°C, 30 s; 59°C, 45 s; 72°C, 1 min), and 72°C, 7 min and (2) *GFAP-cre* by using forward *GFAP-cre* primers (5′-ATGGTCTGGCTCCAGGTACC-3′; Integrated DNA Technologies) and reverse *cre* primers (5′-CAGCATTGCTGTCACTTGGTC-3′; Integrated DNA Technologies) by using the following amplification cycle conditions: 94°C, 3 min; 35 cycles (94°C, 25 s; 59°C, 35 s; 72°C, 45 s); and 72°C, 7 min. Blue/orange 6× loading dye (2 µl; Promega) was added, and 10 ng PCR product was loaded for 1.8% agarose gel electrophoresis in 1× Tris-borate-EDTA buffer. When measured against a 100-bp DNA ladder (Promega), PCR yielded the following bands: 177 bp (wild-type *S1pr1*), 335 bp (floxed *S1pr1*), 450 bp (deletion product), and 625 bp (*Gfap-cre*). Animals with a 450-bp band in ear snip DNA samples indicated germline deletions of S1PR1 and were excluded from breeding and experiments. For each experiment, the heterozygous *S1pr1*$^{fl/+}$*;Gfap-Cre* mice were paired with their heterozygous *S1pr1*$^{fl/+}$ littermates, and their genotypes were blinded to the experimenters.

Immunofluorescence

Immunofluorescence and image analysis was performed by using modifications to previously reported methods (Little et al., 2012; Janes et al., 2014). The spinal cord (L4–6) was harvested, transferred to optimum cutting temperature compound, and rapidly frozen in an isopropanol/dry ice bath. Transverse sections (20 µm) were cut by using a cryostat, collected on gelatin-coated glass microscope slides, and stored at −20°C. Spinal cord sections were fixed in 10% buffered neutral formalin for 10 min (SF100; Thermo Fisher Scientific), blocked (10% normal goat serum 10000C; Thermo Fisher Scientific; 2% BSA, BP9706; Thermo Fisher Scientific; and 0.2% Triton X-100, T8787; Sigma-Aldrich) in PBS (BP39920; Thermo Fisher Scientific) for 1 h and then immunolabeled by using an 18-h incubation (4°C) with mouse monoclonal anti-GFAP antibody, clone G-A-5 (1:200, G3893; Sigma-Aldrich). After a series of PBS rinses, sections were incubated for 2 h with a goat anti–mouse Alexa Fluor 488 antibody (1:250, A-11001; Invitrogen). The coverslips were mounted with Fluorogel II containing DAPI (17985-51; Electron Microscopy Sciences) and photographed with an Olympus FV1000 MPE confocal microscope (multiline argon lasers with excitation at 405 nm and 488 nm) using a 10× objective (UPLSAPO; 0.4 numerical aperture) for regional fluorescence intensity image analysis and with a 60× oil-immersion objective (PLAPONl, 1.42 numerical aperture) and 2.4× optical zoom (0.1-µm pixel dimensions in the X–Y plane and the pinhole set at 1 Airy unit) for higher magnification images. Images were acquired within the dynamic range of the microscope (i.e., no pixel intensity values of 0 or 255 in an 8-bit image). Sections treated with isotype control (X0931; Agilent-Dako) at concentrations equivalent to the primary antibody yielded only nonspecific background fluorescence. Image analysis of GFAP immunolabeling was performed by using the National Institutes of Health freeware program ImageJ (version 1.43; Schneider et al., 2012). The bilateral superficial DHSC (laminae I and II) at the L4, L5, and L6 levels was outlined on images using the ImageJ region of interest tool. The superficial DHSC was determined and confirmed by using adjacent cresyl violet–stained sections and an atlas (Paxinos and Watson, 1998). Images received automated background threshold corrections (histogram-based threshold) before analysis. The mean fluorescence intensity (MFI) of the superficial DHSC was determined as previously reported (Little et al., 2012; Janes et al., 2014). MFI was calculated using the following equation: $MFI = i(pp^2 \div p^2)$, where i is the mean gray value, pp^2 is the positive pixel area, and p^2 is total pixel area. There were no significant differences bilaterally within each group, so MFI was calculated as a combined value for each animal and reported as fold change compared with the vehicle group.

Cytokine assays

Cytokine levels were assessed in DHSC (L4–6) homogenates using a commercially available multiplex cytokine kit (Bio-Rad Laboratories) as previously described (Janes et al., 2014).

In vitro whole-cell recordings and data analysis

Male Sprague Dawley rats (170–180 g) were administered bortezomib (0.2 mg/kg) or its vehicle (5% Tween 80, 5% ethanol in saline) on days 0–4. This resulted in significantly reduced (40.47 ± 8.13%; $P < 0.001$) mechanical PWTs by day 7 with bortezomib treatment. On day 7, traverse L4–5 spinal cord slices were prepared as previously described (Weng et al., 2007; Nie and Weng, 2009). Surgery was performed in deeply isoflurane-anesthetized rats to expose and remove the spinal lumbar enlargement segments. The section was placed in ice-cold sucrose artificial cerebrospinal fluid (234 mM sucrose, 3.6 mM KCl, 1.2 mM $MgCl_2$, 2.5 mM $CaCl_2$, 1.2 mM NaH_2PO_4, 12.0 mM glucose, and 25.0 mM $NaHCO_3$) presaturated with 95% O_2 and 5% CO_2. The pia-arachnoid membrane was removed from the section before it was attached with cyanoacrylate glue to a cutting support and then glued onto the stage of a vibratome (Series 1000; Technical Products International). Transverse spinal cord slices (400 µm) were cut in the ice-cold sucrose artificial cerebrospinal fluid and preincubated in Krebs solution (117.0 mM NaCl, 3.6 mM KCl, 1.2 mM $MgCl_2$, 2.5 mM $CaCl_2$, 1.2 mM NaH_2PO_4, 11.0 mM glucose, and 25.0 mM $NaHCO_3$ at 35°C) oxygenated with 95% O_2 and 5% CO_2 at 35°C. Each single slice was placed in the recording chamber (volume, 1.5 ml), perfused with Krebs solution at 35°C, and saturated with 95% O_2 and 5% CO_2. Borosilicate glass recording electrodes (resistance, 3–5 MΩ) were pulled and filled with an internal solution containing 135 mM potassium-gluconate, 5.0 mM KCl, 2.0 mM $MgCl_2$, 0.5 mM $CaCl_2$, 5.0 mM Hepes, 5.0 mM EGTA, 5.0 mM ATP-Mg, 0.5 mM Na-GTP, and 10 mM QX-314.

Live dorsal horn neurons in the spinal outer lamina II were visualized by microscopy and approached by using a three-dimensional motorized manipulator (Sutter Instrument), and whole-cell configurations were established by applying

moderate negative pressure after electrode contact (Nakatsuka et al., 2003). Recordings of mEPSCs were made from neurons receiving monosynaptic input from the primary afferents by using the criteria established previously (Yoshimura and Jessell, 1989; Weng et al., 2006). mEPSCs were recorded at a membrane potential at −70 mV in the presence of 1 µM tetrodotoxin (T8024; Sigma-Aldrich), 10 µM bicuculline (14340; Sigma-Aldrich), and 5 µM strychnine (S0532; Sigma-Aldrich) in the external solution to block voltage-gated sodium channels, $GABA_A$, and glycine receptors. Data were recorded using Axopatch 700B amplifiers, digitized at 10 kHz, and analyzed off-line. The frequency and amplitude of mEPSCs in 3 min before and during perfusion of tested drugs were analyzed and averaged using a peak detection program (MiniAnalysis; Synaptosoft Inc.).

Tumor cell–killing assays

The effects of FTY720 on the tumor cell toxicity of bortezomib on human multiple myeloma cells (RPMI 8226) was assessed by using an MTT (3-(4,5-dimethylthiazol-2-yl)-2,5-diphenyltetrazolium bromide, M5655; Sigma-Aldrich) assay as previously described (Janes et al., 2013).

Statistical analysis

The data are expressed as mean ± SD or mean ± SEM for *n* animals and analyzed by paired or unpaired *t* test or one-way or two-way repeated-measures ANOVA with Holm-Sidak corrected comparisons. Significant differences were defined as $P < 0.05$, and the false discovery rate for sphingolipid analysis was controlled by Benjamini-Hochberg procedure at $q < 0.05$ using SPSS software (v21; IBM). All other statistical analyses were performed using GraphPad Prism.

Online supplemental material

Fig. S1 shows bortezomib-induced ceramide and dihydroceramide acyl chain species in the spinal cord. Fig. S2 shows the effects of i.th. or oral administration S1PR1-targeted agents on bortezomib-induced mechano-hyperalgesia. Fig. S3 shows the effects of S1PR1-targeted agents on the reversal of established bortezomib-induced mechano-hyperalgesia.

Acknowledgments

We thank Leesa Bryant for her technical assistance in some of the animal experiments.

This work was supported by the Mayday Fund Clinical Evaluation of Novel Biomarkers to Select and Treat Chronic Pain grant, the Leukemia and Lymphoma Society (6241-13 to D. Salvemini and G.J. Bennett), National Institutes of Health (NIH) T32 Training Grant GM008306 (to K. Stockstill, K. Braden, and C.M. Harada), NIH grants RO1NS064289 (to H.-R. Weng) and R01GM043880 (to S. Spiegel), and NIH-National Cancer Institute Cancer Center Support Grant P30 CA016059 (to the Virginia Commonwealth University Lipidomics Core).

D. Salvemini and G.J. Bennett are founders of BioIntervene, Inc., which has licensed related intellectual property from Saint Louis University. All other authors declare no competing financial interests.

Author contributions: K. Stockstill, T.M. Doyle, J.W. Little, K. Janes, Z. Chen, K. Braden, F. Lauro, L.A. Giancotti, C.M. Harada, R. Yadav, and W.H. Xiao performed the experiments. K. Stockstill, T.M. Doyle, and J.W. Little analyzed the data. X. Yan and H.-R. Weng performed the patch-clamp experiments. W.L. Neumann performed the NIBR14 synthesis. S. Spiegel performed the sphingolipidomics. K. Stockstill, T.M. Doyle, J.W. Little, W.L. Neumann, S. Spiegel, J.M. Lionberger, and G.J. Bennett assisted with the manuscript. H.-R. Weng and D. Salvemini wrote the manuscript. D. Salvemini conceived, designed, and led the project.

Submitted: 29 March 2017
Revised: 31 July 2017
Accepted: 21 March 2018

References

Adams, J., V.J. Palombella, E.A. Sausville, J. Johnson, A. Destree, D.D. Lazarus, J. Maas, C.S. Pien, S. Prakash, and P.J. Elliott. 1999. Proteasome inhibitors: a novel class of potent and effective antitumor agents. *Cancer Res.* 59:2615–2622.

Alinari, L., E. Mahoney, J. Patton, X. Zhang, L. Huynh, C.T. Earl, R. Mani, Y. Mao, B. Yu, C. Quinion, et al. 2011. FTY720 increases CD74 expression and sensitizes mantle cell lymphoma cells to milatuzumab-mediated cell death. *Blood.* 118:6893–6903. https://doi.org/10.1182/blood-2011-06-363879

Angst, D., P. Janser, J. Quancard, P. Buehlmayer, F. Berst, L. Oberer, C. Beerli, M. Streiff, C. Pally, R. Hersperger, et al. 2012. An oral sphingosine 1-phosphate receptor 1 (S1P(1)) antagonist prodrug with efficacy in vivo: discovery, synthesis, and evaluation. *J. Med. Chem.* 55:9722–9734. https://doi.org/10.1021/jm3009508

Beider, K., E. Rosenberg, H. Bitner, A. Shimoni, M. Leiba, M. Koren-Michowitz, E. Ribakovsky, S. Klein, D. Olam, L. Weiss, et al. 2017. The sphingosine-1-phosphate modulator FTY720 targets multiple myeloma via the CXCR4/CXCL12 pathway. *Clin. Cancer Res.* 23:1733–1747. https://doi.org/10.1158/1078-0432.CCR-15-2618

Bigaud, M., D. Guerini, A. Billich, F. Bassilana, and V. Brinkmann. 2014. Second generation S1P pathway modulators: research strategies and clinical developments. *Biochim. Biophys. Acta.* 1841:745–758. https://doi.org/10.1016/j.bbalip.2013.11.001

Bolli, M.H., S. Abele, C. Binkert, R. Bravo, S. Buchmann, D. Bur, J. Gatfield, P. Hess, C. Kohl, C. Mangold, et al. 2010. 2-imino-thiazolidin-4-one derivatives as potent, orally active S1P1 receptor agonists. *J. Med. Chem.* 53:4198–4211. https://doi.org/10.1021/jm100181s

Boyette-Davis, J.A., E.T. Walters, and P.M. Dougherty. 2015. Mechanisms involved in the development of chemotherapy-induced neuropathy. *Pain Manag.* 5:285–296. https://doi.org/10.2217/pmt.15.19

Brinkmann, V., A. Billich, T. Baumruker, P. Heining, R. Schmouder, G. Francis, S. Aradhye, and P. Burtin. 2010. Fingolimod (FTY720): discovery and development of an oral drug to treat multiple sclerosis. *Nat. Rev. Drug Discov.* 9:883–897. https://doi.org/10.1038/nrd3248

Carozzi, V.A., C.L. Renn, M. Bardini, G. Fazio, A. Chiorazzi, C. Meregalli, N. Oggioni, K. Shanks, M. Quartu, M.P. Serra, et al. 2013. Bortezomib-induced painful peripheral neuropathy: an electrophysiological, behavioral, morphological and mechanistic study in the mouse. *PLoS One.* 8:e72995. https://doi.org/10.1371/journal.pone.0072995

Chen, D., M. Frezza, S. Schmitt, J. Kanwar, and Q.P. Dou. 2011. Bortezomib as the first proteasome inhibitor anticancer drug: current status and future perspectives. *Curr. Cancer Drug Targets.* 11:239–253. https://doi.org/10.2174/156800911794519752

Chi, X.X., and G.D. Nicol. 2010. The sphingosine 1-phosphate receptor, $S1PR_1$, plays a prominent but not exclusive role in enhancing the excitability of sensory neurons. *J. Neurophysiol.* 104:2741–2748. https://doi.org/10.1152/jn.00709.2010

Choi, J.W., S.E. Gardell, D.R. Herr, R. Rivera, C.W. Lee, K. Noguchi, S.T. Teo, Y.C. Yung, M. Lu, G. Kennedy, and J. Chun. 2011. FTY720 (fingolimod) efficacy in an animal model of multiple sclerosis requires astrocyte sphingosine 1-phosphate receptor 1 (S1P1) modulation. *Proc. Natl. Acad. Sci. USA.* 108:751–756. https://doi.org/10.1073/pnas.1014154108

Clark, A.K., E.A. Old, and M. Malcangio. 2013. Neuropathic pain and cytokines: current perspectives. *J. Pain Res.* 6:803–814.

Dawkins, J.L., D.J. Hulme, S.B. Brahmbhatt, M. Auer-Grumbach, and G.A. Nicholson. 2001. Mutations in SPTLC1, encoding serine palmitoyltransferase, long chain base subunit-1, cause hereditary sensory neuropathy type I. *Nat. Genet.* 27:309–312. https://doi.org/10.1038/85879

Delgado, A., J. Casas, A. Llebaria, J.L. Abad, and G. Fabrias. 2006. Inhibitors of sphingolipid metabolism enzymes. *Biochim. Biophys. Acta.* 1758:1957–1977. https://doi.org/10.1016/j.bbamem.2006.08.017

de Moor, J.S., A.B. Mariotto, C. Parry, C.M. Alfano, L. Padgett, E.E. Kent, L. Forsythe, S. Scoppa, M. Hachey, and J.H. Rowland. 2013. Cancer survivors in the United States: prevalence across the survivorship trajectory and implications for care. *Cancer Epidemiol. Biomarkers Prev.* 22:561–570. https://doi.org/10.1158/1055-9965.EPI-12-1356

Dixon, W.J. 1980. Efficient analysis of experimental observations. *Annu. Rev. Pharmacol. Toxicol.* 20:441–462. https://doi.org/10.1146/annurev.pa.20.040180.002301

Duggett, N.A., and S.J.L. Flatters. 2017. Characterization of a rat model of bortezomib-induced painful neuropathy. *Br. J. Pharmacol.* 174:4812–4825. https://doi.org/10.1111/bph.14063

Farquhar-Smith, P. 2011. Chemotherapy-induced neuropathic pain. *Curr. Opin. Support. Palliat. Care.* 5:1–7. https://doi.org/10.1097/SPC.0b013e328342f9cc

Ghelardini, C., C. Menicacci, D. Cerretani, and E. Bianchi. 2014. Spinal administration of mGluR5 antagonist prevents the onset of bortezomib induced neuropathic pain in rat. *Neuropharmacology.* 86:294–300. https://doi.org/10.1016/j.neuropharm.2014.08.004

Gong, L., B. Yang, M. Xu, B. Cheng, X. Tang, P. Zheng, Y. Jing, and G.J. Wu. 2014. Bortezomib-induced apoptosis in cultured pancreatic cancer cells is associated with ceramide production. *Cancer Chemother. Pharmacol.* 73:69–77. https://doi.org/10.1007/s00280-013-2318-3

Hait, N.C., J. Allegood, M. Maceyka, G.M. Strub, K.B. Harikumar, S.K. Singh, C. Luo, R. Marmorstein, T. Kordula, S. Milstien, and S. Spiegel. 2009. Regulation of histone acetylation in the nucleus by sphingosine-1-phosphate. *Science.* 325:1254–1257. https://doi.org/10.1126/science.1176709

Hait, N.C., D. Avni, A. Yamada, M. Nagahashi, T. Aoyagi, H. Aoki, C.I. Dumur, Z. Zelenko, E.J. Gallagher, D. Leroith, et al. 2015. The phosphorylated prodrug FTY720 is a histone deacetylase inhibitor that reactivates ERα expression and enhances hormonal therapy for breast cancer. *Oncogenesis.* 4:e156. https://doi.org/10.1038/oncsis.2015.16

Han, Y., and M.T. Smith. 2013. Pathobiology of cancer chemotherapy-induced peripheral neuropathy (CIPN). *Front. Pharmacol.* 4:156. https://doi.org/10.3389/fphar.2013.00156

Hannun, Y.A., and L.M. Obeid. 2008. Principles of bioactive lipid signalling: lessons from sphingolipids. *Nat. Rev. Mol. Cell Biol.* 9:139–150. https://doi.org/10.1038/nrm2329

Janes, K., T. Doyle, L. Bryant, E. Esposito, S. Cuzzocrea, J. Ryerse, G.J. Bennett, and D. Salvemini. 2013. Bioenergetic deficits in peripheral nerve sensory axons during chemotherapy-induced neuropathic pain resulting from peroxynitrite-mediated post-translational nitration of mitochondrial superoxide dismutase. *Pain.* 154:2432–2440. https://doi.org/10.1016/j.pain.2013.07.032

Janes, K., J.W. Little, C. Li, L. Bryant, C. Chen, Z. Chen, K. Kamocki, T. Doyle, A. Snider, E. Esposito, et al. 2014. The development and maintenance of paclitaxel-induced neuropathic pain require activation of the sphingosine 1-phosphate receptor subtype 1. *J. Biol. Chem.* 289:21082–21097. https://doi.org/10.1074/jbc.M114.569574

Kawasaki, Y., L. Zhang, J.K. Cheng, and R.R. Ji. 2008. Cytokine mechanisms of central sensitization: distinct and overlapping role of interleukin-1beta, interleukin-6, and tumor necrosis factor-alpha in regulating synaptic and neuronal activity in the superficial spinal cord. *J. Neurosci.* 28:5189–5194. https://doi.org/10.1523/JNEUROSCI.3338-07.2008

Kim, S., A.J. Steelman, Y. Zhang, H.C. Kinney, and J. Li. 2012. Aberrant upregulation of astroglial ceramide potentiates oligodendrocyte injury. *Brain Pathol.* 22:41–57. https://doi.org/10.1111/j.1750-3639.2011.00501.x

Liang, Y., S. Ma, Y. Zhang, Y. Wang, Q. Cheng, Y. Wu, Y. Jin, D. Zheng, D. Wu, and H. Liu. 2014. IL-1β and TLR4 signaling are involved in the aggravated murine acute graft-versus-host disease caused by delayed bortezomib administration. *J. Immunol.* 192:1277–1285. https://doi.org/10.4049/jimmunol.1203428

Lissin, D.V., R.C. Carroll, R.A. Nicoll, R.C. Malenka, and M. von Zastrow. 1999. Rapid, activation-induced redistribution of ionotropic glutamate receptors in cultured hippocampal neurons. *J. Neurosci.* 19:1263–1272. https://doi.org/10.1523/JNEUROSCI.19-04-01263.1999

Little, J.W., Z. Chen, T. Doyle, F. Porreca, M. Ghaffari, L. Bryant, W.L. Neumann, and D. Salvemini. 2012. Supraspinal peroxynitrite modulates pain signaling by suppressing the endogenous opioid pathway. *J. Neurosci.* 32:10797–10808. https://doi.org/10.1523/JNEUROSCI.6345-11.2012

Maceyka, M., and S. Spiegel. 2014. Sphingolipid metabolites in inflammatory disease. *Nature.* 510:58–67. https://doi.org/10.1038/nature13475

Mullershausen, F., L.M. Craveiro, Y. Shin, M. Cortes-Cros, F. Bassilana, M. Osinde, W.L. Wishart, D. Guerini, M. Thallmair, M.E. Schwab, et al. 2007. Phosphorylated FTY720 promotes astrocyte migration through sphingosine-1-phosphate receptors. *J. Neurochem.* 102:1151–1161. https://doi.org/10.1111/j.1471-4159.2007.04629.x

Muscoli, C., T. Doyle, C. Dagostino, L. Bryant, Z. Chen, L.R. Watkins, J. Ryerse, E. Bieberich, W. Neumman, and D. Salvemini. 2010. Counter-regulation of opioid analgesia by glial-derived bioactive sphingolipids. *J. Neurosci.* 30:15400–15408. https://doi.org/10.1523/JNEUROSCI.2391-10.2010

Nakatsuka, T., K. Tsuzuki, J.X. Ling, H. Sonobe, and J.G. Gu. 2003. Distinct roles of P2X receptors in modulating glutamate release at different primary sensory synapses in rat spinal cord. *J. Neurophysiol.* 89:3243–3252. https://doi.org/10.1152/jn.01172.2002

Neviani, P., J.G. Harb, J.J. Oaks, R. Santhanam, C.J. Walker, J.J. Ellis, G. Ferenchak, A.M. Dorrance, C.A. Paisie, A.M. Eiring, et al. 2013. PP2A-activating drugs selectively eradicate TKI-resistant chronic myeloid leukemic stem cells. *J. Clin. Invest.* 123:4144–4157. https://doi.org/10.1172/JCI68951

Nie, H., and H.R. Weng. 2009. Glutamate transporters prevent excessive activation of NMDA receptors and extrasynaptic glutamate spillover in the spinal dorsal horn. *J. Neurophysiol.* 101:2041–2051. https://doi.org/10.1152/jn.91138.2008

O'Sullivan, S., and K.K. Dev. 2017. Sphingosine-1-phosphate receptor therapies: Advances in clinical trials for CNS-related diseases. *Neuropharmacology.* 113(Pt B):597–607. https://doi.org/10.1016/j.neuropharm.2016.11.006

Ogretmen, B., and Y.A. Hannun. 2004. Biologically active sphingolipids in cancer pathogenesis and treatment. *Nat. Rev. Cancer.* 4:604–616. https://doi.org/10.1038/nrc1411

Paxinos, G., and C. Watson. 1998. The rat brain in stereotaxic coordinates. Academic Press, San Diego.

Robinson, C.R., H. Zhang, and P.M. Dougherty. 2014. Astrocytes, but not microglia, are activated in oxaliplatin and bortezomib-induced peripheral neuropathy in the rat. *Neuroscience.* 274:308–317. https://doi.org/10.1016/j.neuroscience.2014.05.051

Rothhammer, V., J.E. Kenison, E. Tjon, M.C. Takenaka, K.A. de Lima, D.M. Borucki, C.C. Chao, A. Wilz, M. Blain, L. Healy, et al. 2017. Sphingosine 1-phosphate receptor modulation suppresses pathogenic astrocyte activation and chronic progressive CNS inflammation. *Proc. Natl. Acad. Sci. USA.* 114:2012–2017. https://doi.org/10.1073/pnas.1615413114

Salvemini, D., T. Doyle, M. Kress, and G. Nicol. 2013. Therapeutic targeting of the ceramide-to-sphingosine 1-phosphate pathway in pain. *Trends Pharmacol. Sci.* 34:110–118. https://doi.org/10.1016/j.tips.2012.12.001

Schneider, C.A., W.S. Rasband, and K.W. Eliceiri. 2012. NIH Image to ImageJ: 25 years of image analysis. *Nat. Methods.* 9:671–675. https://doi.org/10.1038/nmeth.2089

Sennepin, A.D., S. Charpentier, T. Normand, C. Sarré, A. Legrand, and L.M. Mollet. 2009. Multiple reprobing of Western blots after inactivation of peroxidase activity by its substrate, hydrogen peroxide. *Anal. Biochem.* 393:129–131. https://doi.org/10.1016/j.ab.2009.06.004

Seruga, B., H. Zhang, L.J. Bernstein, and I.F. Tannock. 2008. Cytokines and their relationship to the symptoms and outcome of cancer. *Nat. Rev. Cancer.* 8:887–899. https://doi.org/10.1038/nrc2507

Siau, C., W. Xiao, and G.J. Bennett. 2006. Paclitaxel- and vincristine-evoked painful peripheral neuropathies: loss of epidermal innervation and activation of Langerhans cells. *Exp. Neurol.* 201:507–514. https://doi.org/10.1016/j.expneurol.2006.05.007

Snider, A.J., K.A. Orr Gandy, and L.M. Obeid. 2010. Sphingosine kinase: Role in regulation of bioactive sphingolipid mediators in inflammation. *Biochimie.* 92:707–715. https://doi.org/10.1016/j.biochi.2010.02.008

Sorensen, S.D., O. Nicole, R.D. Peavy, L.M. Montoya, C.J. Lee, T.J. Murphy, S.F. Traynelis, and J.R. Hepler. 2003. Common signaling pathways link activation of murine PAR-1, LPA, and S1P receptors to proliferation of astrocytes. *Mol. Pharmacol.* 64:1199–1209. https://doi.org/10.1124/mol.64.5.1199

Spiegel, S., and S. Milstien. 2011. The outs and the ins of sphingosine-1-phosphate in immunity. *Nat. Rev. Immunol.* 11:403–415. https://doi.org/10.1038/nri2974

Strub, G.M., M. Maceyka, N.C. Hait, S. Milstien, and S. Spiegel. 2010. Extracellular and intracellular actions of sphingosine-1-phosphate. *Adv. Exp. Med. Biol.* 688:141–155. https://doi.org/10.1007/978-1-4419-6741-1_10

Walk, R.M., S.T. Elliott, F.C. Blanco, J.A. Snyder, A.M. Jacobi, S.D. Rose, M.A. Behlke, A.K. Salem, S. Vukmanovic, and A.D. Sandler. 2012. T-cell activation is enhanced by targeting IL-10 cytokine production in toll-like receptor-stimulated macrophages. *ImmunoTargets Ther.* 1:13–23.

Weng, H.R., J.H. Chen, and J.P. Cata. 2006. Inhibition of glutamate uptake in the spinal cord induces hyperalgesia and increased responses of spinal dorsal horn neurons to peripheral afferent stimulation. *Neuroscience.* 138:1351–1360. https://doi.org/10.1016/j.neuroscience.2005.11.061

Weng, H.R., J.H. Chen, Z.Z. Pan, and H. Nie. 2007. Glial glutamate transporter 1 regulates the spatial and temporal coding of glutamatergic synaptic transmission in spinal lamina II neurons. *Neuroscience.* 149:898–907. https://doi.org/10.1016/j.neuroscience.2007.07.063

White, C., H. Alshaker, C. Cooper, M. Winkler, and D. Pchejetski. 2016. The emerging role of FTY720 (Fingolimod) in cancer treatment. *Oncotarget.* 7:23106–23127. https://doi.org/10.18632/oncotarget.7145

Yan, X., and H.R. Weng. 2013. Endogenous interleukin-1β in neuropathic rats enhances glutamate release from the primary afferents in the spinal dorsal horn through coupling with presynaptic N-methyl-D-aspartic acid receptors. *J. Biol. Chem.* 288:30544–30557. https://doi.org/10.1074/jbc.M113.495465

Yan, X., E. Jiang, M. Gao, and H.R. Weng. 2013. Endogenous activation of presynaptic NMDA receptors enhances glutamate release from the primary afferents in the spinal dorsal horn in a rat model of neuropathic pain. *J. Physiol.* 591:2001–2019. https://doi.org/10.1113/jphysiol.2012.250522

Yarlagadda, A., E. Alfson, and A.H. Clayton. 2009. The blood brain barrier and the role of cytokines in neuropsychiatry. *Psychiatry (Edgmont Pa.).* 6:18–22.

Yasui, H., T. Hideshima, N. Raje, A.M. Roccaro, N. Shiraishi, S. Kumar, M. Hamasaki, K. Ishitsuka, Y.T. Tai, K. Podar, et al. 2005. FTY720 induces apoptosis in multiple myeloma cells and overcomes drug resistance. *Cancer Res.* 65:7478–7484. https://doi.org/10.1158/0008-5472.CAN-05-0850

Yoshimura, M., and T.M. Jessell. 1989. Primary afferent-evoked synaptic responses and slow potential generation in rat substantia gelatinosa neurons in vitro. *J. Neurophysiol.* 62:96–108. https://doi.org/10.1152/jn.1989.62.1.96

Zhang, Y., K. Chen, S.A. Sloan, M.L. Bennett, A.R. Scholze, S. O'Keeffe, H.P. Phatnani, P. Guarnieri, C. Caneda, N. Ruderisch, et al. 2014. An RNA-sequencing transcriptome and splicing database of glia, neurons, and vascular cells of the cerebral cortex. *J. Neurosci.* 34:11929–11947. https://doi.org/10.1523/JNEUROSCI.1860-14.2014

Zheng, H., W.H. Xiao, and G.J. Bennett. 2012. Mitotoxicity and bortezomib-induced chronic painful peripheral neuropathy. *Exp. Neurol.* 238:225–234. https://doi.org/10.1016/j.expneurol.2012.08.023